

pubs.acs.org/JPCL Letter

S2 Subunit of SARS-CoV-2 Spike Protein Induces Domain Fusion in Natural Pulmonary Surfactant Monolayers

Xiaojie Xu, Guangle Li, Bingbing Sun, and Yi Y. Zuo*



Cite This: J. Phys. Chem. Lett. 2022, 13, 8359-8364



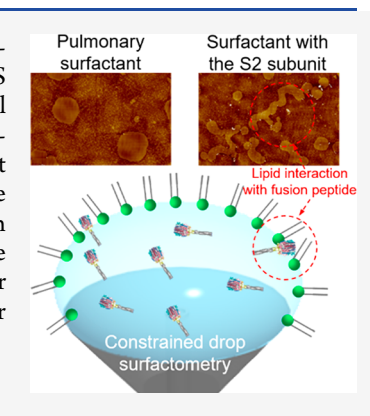
ACCESS I

III Metrics & More

Article Recommendations

Supporting Information

ABSTRACT: Pulmonary surfactant has been attempted as a supportive therapy to treat COVID-19. Although it is mechanistically accepted that the fusion peptide in the S2 subunit of the S protein plays a predominant role in mediating viral fusion with the host cell membrane, it is still unknown how the S2 subunit interacts with the natural surfactant film. Using combined bio-physicochemical assays and atomic force microscopy imaging, it was found that the S2 subunit inhibited the biophysical properties of the surfactant and induced microdomain fusion in the surfactant monolayer. The surfactant inhibition has been attributed to membrane fluidization caused by insertion of the S2 subunit mediated by its fusion peptide. These findings may provide novel insight into the understanding of bio-physicochemical mechanisms responsible for surfactant interactions with SARS-CoV-2 and may have translational implications in the further development of surfactant replacement therapy for COVID-19 patients.



S evere acute respiratory syndrome coronavirus 2 (SARS-CoV-2), the virus responsible for coronavirus disease 2019 (COVID-19), is causing a global pandemic with millions of deaths. SARS-CoV-2 is an enveloped, positive-sense, single-stranded RNA virus with a genome size of $\sim 30~\text{kb.}^1$ It consists of four structural proteins, namely, nucleocapsid (N), membrane (M), envelope (E), and spike (S). Among these proteins, the S protein is the major mediator of cellular infection, which determines the attachment of SARS-CoV-2 onto the host cell membrane and the subsequent membrane fusion. During infection, the S protein recognizes and binds to angiotensin-converting enzyme 2 (ACE2) on the host cell membrane and thus mediates viral cellular entry.

The S protein is a heavily glycosylated, trimeric, type I membrane protein anchored on the exterior surface of the mature virion.³ Each monomer of the trimeric S protein is about 180 kDa with 1273 amino acids. It is composed of a signal peptide (residues 1-13) and two functional subunits, that is, the S1 subunit (residues 14-685) responsible for binding to the host cell receptor and the S2 subunit (residues 686-1273) responsible for fusion of the viral and cellular membranes.⁴ Once bound to the cell membrane, the S protein undergoes cleavage by proteases, such as furin, into the S1 and S2 subunits. 5 As illustrated in Figure 1A, the S1 subunit consists of an N-terminal domain and a receptor-binding domain that interacts with ACE2. The S2 subunit consists of a fusion peptide, central helix, connecting domain, heptad repeat 1 and 2, transmembrane domain, and cytoplasmic tail (Figure 1A,B). After S protein cleavage and membrane fusion, a fusion pore forms between viral and cellular membranes, which facilitates delivery of the viral genetic information into the host cell cytoplasm for further replication and transcription.

In COVID-19-associated acute respiratory distress syndrome (ARDS),6 SARS-CoV-2 attacks alveolar epithelial cells, where the ACE2 receptor is highly expressed. Damage to type II alveolar epithelial cells could compromise the synthesis and function of the endogenous pulmonary surfactant (PS) that plays a crucial physiological role in host defense and alveolar surface tension reduction. The PS is composed of ~80 wt % phospholipids, with dipalmitoylphosphatidylcholine (DPPC) being the major lipid species, ~10 wt % cholesterol, and ~10 wt % surfactant-associated proteins SP-A, -B, -C, and -D. SP-A and SP-D, presenting in airways and the alveolar regions, were found to bind to the S protein, thus mitigating infection of the epithelial cells through viral neutralization, agglutination, and enhanced phagocytosis.^{9,10} In addition, a recent clinical trial showed that the DPPC levels in the bronchoalveolar lavage fluids of COVID-19 patients were lower than those in healthy controls. 11 All this evidence justified the hypothesis that exogenous surfactant therapy, in which clinical surfactant preparations extracted from animals' lungs are delivered to patients' lungs, may be used as a supportive therapy to treat patients with COVID-19 and COVID-19-associated ARDS. 12-14 There have been multiple

Received: June 28, 2022 Accepted: August 29, 2022



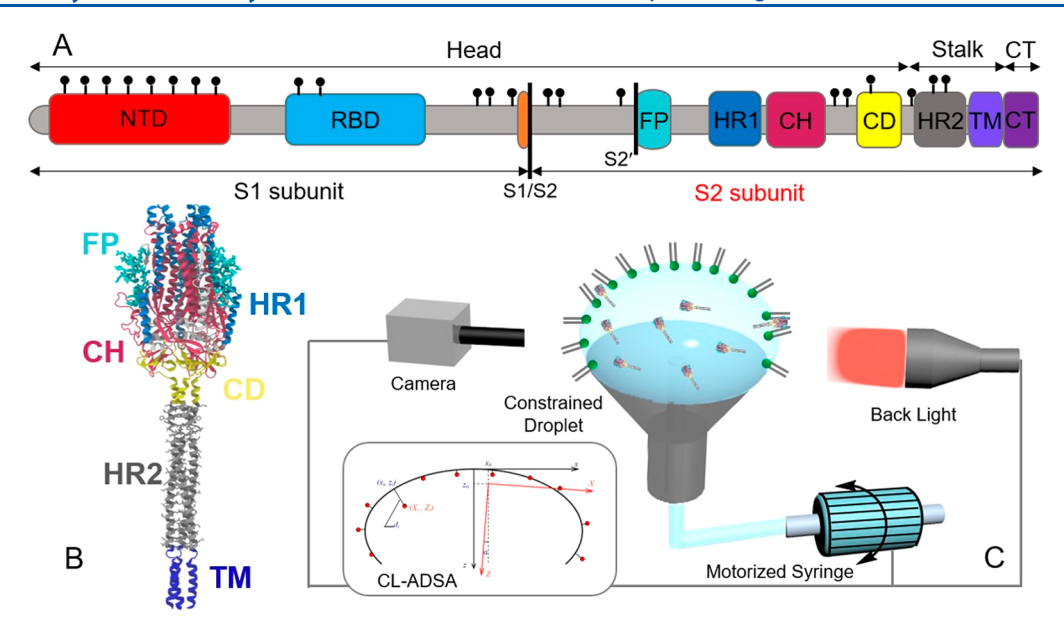


Figure 1. (A) Primary structure of the SARS-CoV-2 S protein. It is composed of the S1 and S2 subunits. The S1 subunit contains an N-terminal domain (NTD) and a receptor-binding domain (RBD). The S2 subunit consists of a fusion peptide (FP), central helix (CH), connecting domain (CD), heptad repeat 1 (HR1) and 2 (HR2), transmembrane (TM) domain, and cytoplasmic tail (CT). (B) Cryo-EM structures of the S2 subunit from the Protein Data Bank ID 6VXX. (C) Constrained drop surfactometry (CDS) for probing biophysical interactions between natural pulmonary surfactant and the S2 subunit.

ongoing clinical trials in the past two years.¹⁴ Although the verdict is still out, preliminary reports have demonstrated promise for the surfactant therapy in managing the progress of COVID-19.^{15,16}

Clinical application of the exogenous surfactant therapy in COVID-19 entails a biophysical understanding of specific interactions between the PS film and the functional group of SARS-CoV-2 responsible for mediating membrane fusion. It is mechanistically accepted that the fusion peptide (FP) in the S2 subunit of the S protein takes a central role in mediating the initial penetration of the virus into the host cell membrane. There have been a few in silico studies based on molecular dynamics simulations that investigated the specific FP-lipid interactions in the initial stage of SARS-CoV-2 infection. However, it is still unknown how the FP of the S2 subunit interacts with or adversely impacts the natural PS film.

Here, we experimentally studied the specific biophysical interactions between the recombinant S2 subunit and an animal-derived clinical surfactant, that is, Infasurf, using constrained drop surfactometry (CDS) (Figure 1C). With biophysical simulations using CDS and molecular visualization using atomic force microscopy (AFM), we found that the S2 subunit inhibited the biophysical properties of PS and, most importantly, directly induced fusion of phospholipid microdomains in the Infasurf monolayer. These results may provide novel insight into the understanding of biophysical mechanisms responsible for PS interactions with SARS-CoV-2 and may have translational implications in further developing the surfactant replacement therapy for COVID-19 patients.

Figure 2 shows the biophysical impact of the S2 subunit on the Infasurf film under physiologically relevant conditions. Reproducibility is demonstrated in Figure S1 of the Supporting Information. The surface area of the Infasurf film was oscillated with a 20% compression ratio (CR) and a highly dynamic rate of 3 s per compression—expansion cycle, to mimic breathing.²³

Figure 2A shows cycles of 1 mg/mL Infasurf with a low 0.15 mol % or a moderate 0.75 mol % S2 subunit. The minimum surface tension ($\gamma_{\rm min}$) of Infasurf is increased from 2.9 to 4.4 mN/m with 0.15% S2 subunit and to 6.5 mN/m with 0.75% S2 subunit, indicating significant surfactant inhibition (Figure 2B). The compressibility ($\kappa_{\rm comp}$) of the Infasurf film is increased from 0.64 to 0.71 m/mN with 0.75% S2 subunit (Figure 2C). The film compressibility is a quantitative measure of the "softness" of the PS film. The increase of film compressibility is an indication of the strong implication of biophysical inhibition of the PS, since more area reduction is needed to decrease the surface tension.

Other than the physiologically relevant 20% CR, dynamic surface activities of the Infasurf film were also studied at supraphysiological levels of 30% and 40% CRs (Figure 2D–I). Similar to 20% CR, the addition of 0.75% S2 subunit more than doubles the corresponding $\gamma_{\rm min}$ and $\kappa_{\rm comp}$ of the Infasurf film, thus indicating significant biophysical inhibition of the PS function.

Figure 3 demonstrates the isothermal compression of Infasurf at a quasi-static rate of 0.1 cm²/min, with and without S2 subunit injected into the subphase, that is, the droplet, to a protein concentration of 0.05 mg/mL. The compression isotherms of the Infasurf monolayer with a faster compression of 0.3 cm²/min and with a higher S2 concentration of 0.1 mg/ mL were also studied (Figure S2). It can be seen that, at two temperatures—20 and 37 °C—the S2 subunit injected into the subphase significantly increases the initial surface pressure prior to monolayer compression, to the surface pressure of $\sim 20 \text{ mN}/$ m, corresponding to the S2 subunit's equilibrium surface tension at 50 mN/m (see Figure S3 for adsorption kinetics of the S2 subunit). At both temperatures, the compression isotherms reach a plateau region at the equilibrium spreading pressure (π_{eq}) of surfactant at 50 mN/m, where the PS monolayer is transformed into a multilayer. 24,25 While the Infasurf monolayer at 20 °C can be further compressed to a

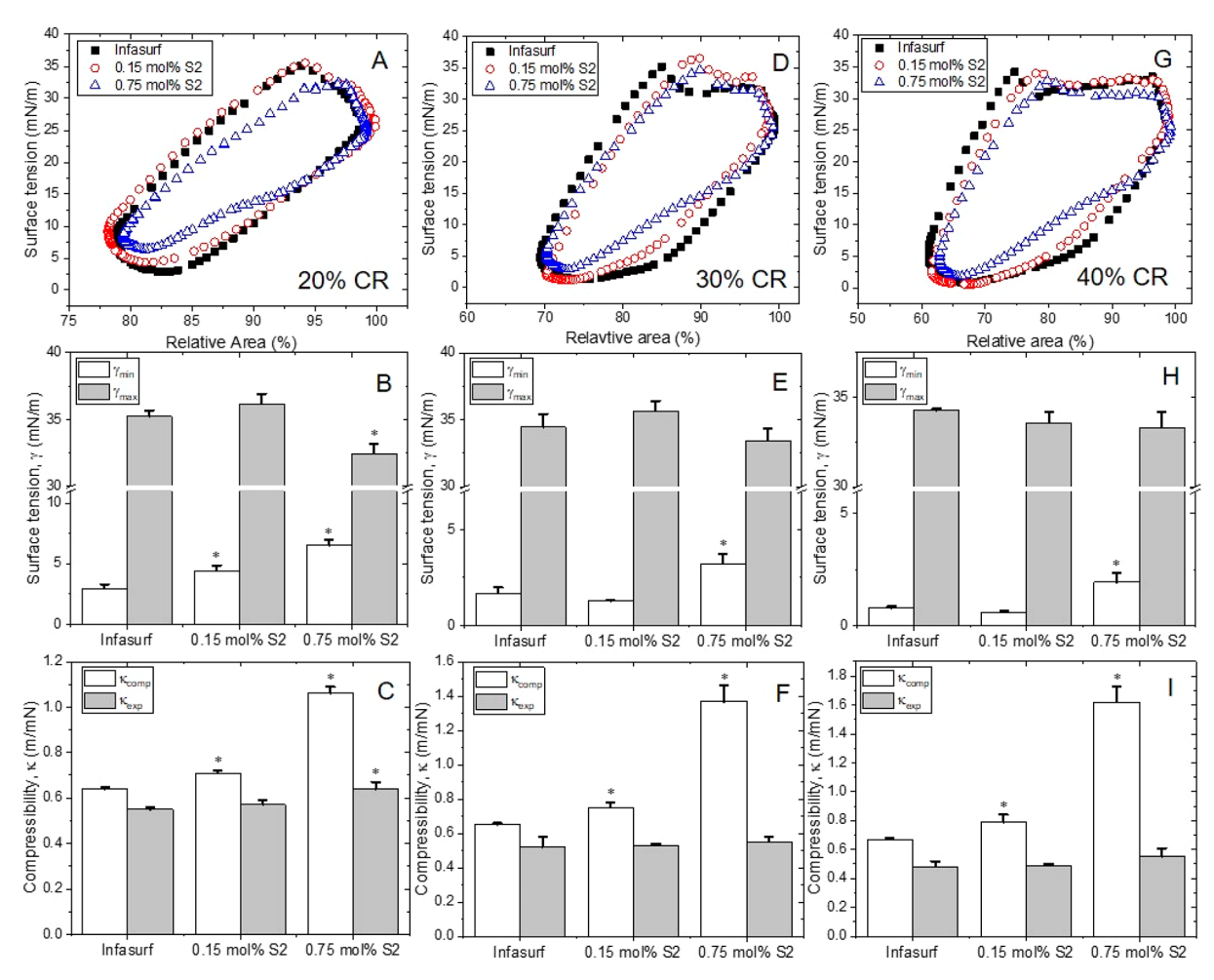


Figure 2. Effect of the S2 subunit (0.15 and 0.75 mol %) on the biophysical properties of 1 mg/mL Infasurf, with various compression ratios (CRs). (A–C) 20% CR, (D–F) 30% CR, and (G–I) 40% CR. (A, D, G) show the dynamic compression–expansion cycles of Infasurf with/without the S subunit. (B, E, H) show the statistical analysis of γ_{\min} and maximum surface tension (γ_{\max}). (C, F, I) show the analysis of κ_{comp} and the compressibility for the expansion process (κ_{exp}). Results shown are the tenth cycle. *p < 0.05 suggests statistically significant differences in comparison to pure Infasurf film without the S2 subunit.

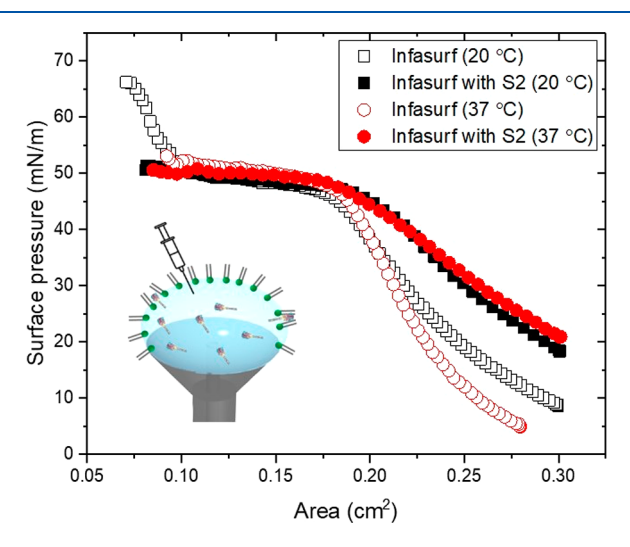


Figure 3. Effect of the S2 subunit on the quasi-static compression isotherms of spread Infasurf monolayers. Aqueous solution of the S2 subunit was subphase injected to a protein concentration of 0.05 mg/mL *prior to* monolayer compression. The Infasurf monolayer was quasi-statically compressed at a rate of 0.1 cm²/min, under two environmental temperatures of 20 and 37 °C.

metastable supracompressed state above the $\pi_{\rm eq}^{24,26}$ the Infasurf monolayer with the subphase-injected S2 subunit spontaneously collapses at $\pi_{\rm eq}$ thus indicating the S2 subunit-induced surfactant inhibition.

Figure 4 shows AFM topographic images of Infasurf at the characteristic surface pressure of 30 mN/m, with/without the S2 subunit under two environmental temperatures of 20 and 37 °C, respectively. Figures S4–S7 show the reproducibility of these images. At 20 °C (Figure 4A), the Infasurf monolayer shows microscale and nanoscale tilted-condensed (TC) domains that are approximately 0.8–1.0 nm higher than the liquid-expanded (LE) phase, which is mostly composed of fluid phospholipids. These TC domains mainly contain solid-like disaturated phospholipids, largely DPPC. These microdomains have a nearly circular shape with a diameter of 3–5 μ m, in good agreement with our previous observations.²⁴

Addition of the S2 subunit completely alters the lateral structure of the Infasurf monolayer. The most striking change caused by the S2 subunit is the morphology of the microdomains. As shown in Figure 4B, the microdomains, ~1 nm higher than the LE phase, mostly merge into an irregular wormlike shape. A small amount of isolated circular microdomains still appears in the monolayer but exists with a much smaller diameter than that of the Infasurf monolayer (1.5

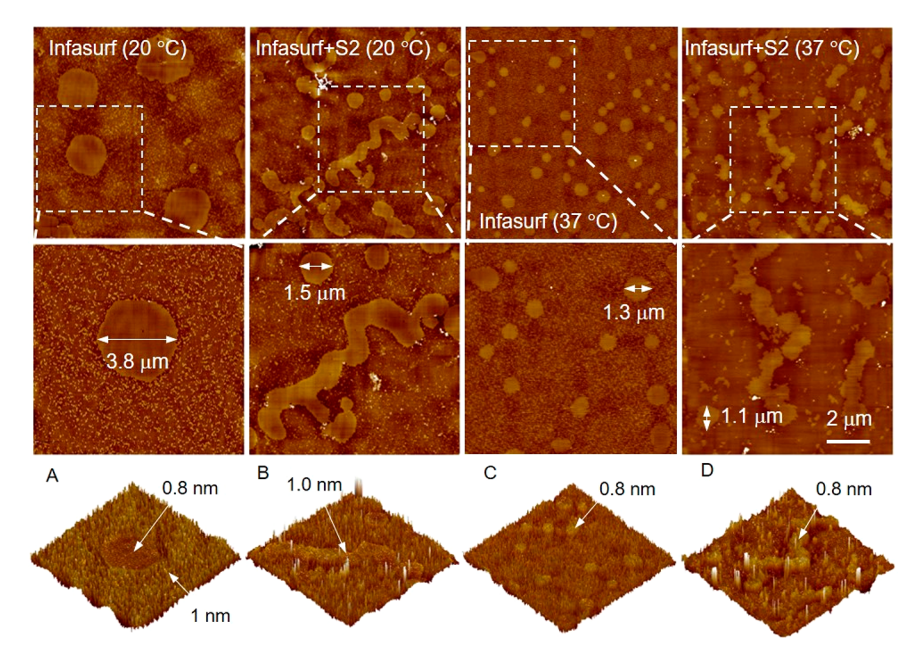


Figure 4. AFM images of Infasurf with/without the addition of the S2 subunit, under two environmental temperatures of 20 and 37 °C, respectively. (A) Infasurf at 20 °C, (B) Infasurf with S2 at 20 °C, (C) Infasurf at 37 °C, and (D) Infasurf with S2 at 37 °C. All AFM images were obtained at the characteristic surface pressure of 30 mN/m. AFM images in the first row are $20 \times 20 \,\mu\text{m}$ in the lateral dimension and 5 nm in the z range. Images in the middle row demonstrate the enlarged structures in the white boxes. The bottom row shows the 3D renderings of the topographic images shown in the middle row. White arrows point to designated lateral and altitudinal dimensions.

vs 3.8 μ m). A similar effect of the S2 subunit on the Infasurf monolayer is also found at 37 °C. As shown in Figure 4C, microdomains of the Infasurf monolayer at 37 °C are, in general, smaller than those at 20 °C (1.3 vs 3.8 μ m). A subphase-injected S2 subunit also causes fusion of microdomains in the Infasurf monolayer at 37 °C (Figure 4D).

Figure 5 shows the quantified domain coverage of the Infasurf monolayer. In general, addition of the S2 subunit

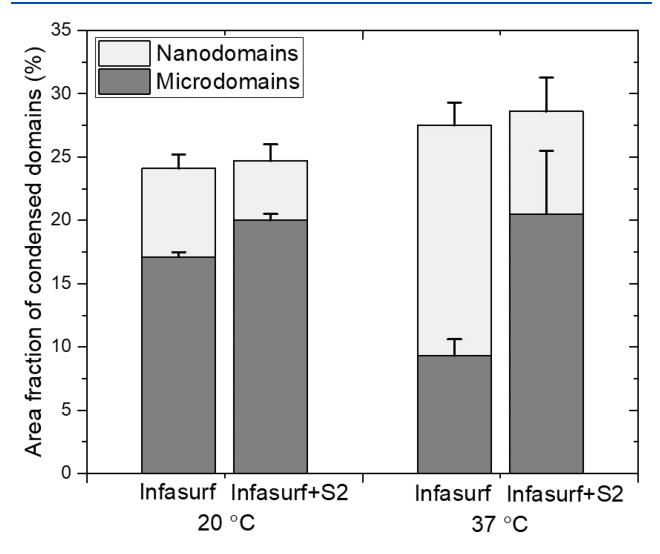


Figure 5. Quantification results for the Infasurf monolayer coverage of TC microdomains and nanodomains at surface pressure 30 mN/m.

increases the area fraction of microdomains but decreases the area fraction of the nanodomains. However, the total area fraction of microdomains and nanodomains remains at around 25–30% and does not appear to change with the addition of the S2 subunit. Infasurf contains a total of approximately 40%

disaturated phospholipids, mostly DPPC.²⁴ Therefore, it appears that the lipid composition of the Infasurf monolayer, with and without the S2 subunit, is close to that of Infasurf. Hence, the S2 subunit only varies the domain morphology by inducing domain fusion, instead of changing the lipid composition of the natural PS film.

The equilibrium morphology of microdomains of phospholipid monolayers is controlled by competition of line tension at the domain boundaries and electrostatic repulsion between lipid headgroups in the domain. A large line tension favors the formation of a small number of larger domains with a round shape, thus minimizing the total domain boundaries. This mechanism explains why the size of microdomains in the Infasurf monolayer at 37 °C is much smaller than that at 20 °C (Figure 4A vs C), because, in general, line tension decreases with temperature.

The dramatic change of microdomain morphology with the addition of the S2 subunit (Figure 4A vs B and Figure 4C vs D) must be caused by a significantly reduced line tension at the domain boundary. It is not unexpected that the fusion peptide of the S2 subunit selectively partitions into the microdomain boundaries to reduce line tension. It has been proposed that line tension dominates the human immunodeficiency virus (HIV) FP-mediated fusion. Since the solid-like domains mostly consist of ordered lipid phases, they are energetically unfavorable for membrane fusion when it comes to infection by enveloped viruses, such as HIV and influenza. It has been found that line tension induces HIV gp41-FP-mediated fusion. Similarly, line tension was found to be a significant control factor for membrane fusion mediated by influenza hemagglutinin.

A critical stage of viral infection is the fusion between viral and host cell membranes. The FP of the S2 subunit is responsible for the initial penetration of the virus into the host cell membrane.²⁹ The FP is a relatively hydrophobic residue

located at the N-terminus of the S2 subunit. Molecular dynamics simulations have shown that residues L821, L822, and F823 in the helical portion of the FP can deeply insert into the hydrophobic core of a model membrane, thus closely interacting with the membrane lipids. Other hydrophobic residues of the FP may also contribute to binding to biomembrane, thus minimizing its exposure to water. Once bound to the membrane, a fully conserved disulfide bridge in the FP establishes the strong anchoring that is required for subsequent membrane fusion.

In comparison to extensive studies of the FP-mediated membrane fusion, it is still unknown how the FP of an enveloped virus affects the natural PS film. The endogenous PS film adsorbed at the alveolar surface is a lipid—protein biomembrane that consists of an interfacial monolayer with functionally attached multilayers composed of hundreds of fluid phospholipids. In terms of membrane structures, the PS monolayer controlled at the surface pressure 30 mN/m can be loosely considered as a natural model mimicking a single leaflet of a biomembrane, since the lateral pressure of enclosed bilayers is largely conserved at 30 mN/m.

Using combined biophysical simulations with CDS and direct membrane imaging with AFM, we have established two experimental findings. First, the S2 subunit at a molar ratio of 0.75% with respect to phospholipids strongly inhibited the biophysical function of a natural PS (Figure 2). Second, the S2 subunit subphase injected at a low concentration of 0.05 mg/mL induced significant domain fusion in the natural PS monolayer (Figure 4). These two biophysical findings are interrelated, since the membrane fluidization caused by the penetration of the S2 subunit is most likely responsible for the surfactant inhibition as revealed by the increase of film compressibility.

It has been shown that the FP of the S2 subunit transforms from an intrinsically disordered state in an aqueous solution into a wedge-shaped structure inserting into bilayered micelles, with the hydrophobic, narrow end of the wedge contacting the fatty acyl chains of the phospholipids and the polar end of the wedge interacting with the lipid head groups and binding calcium ions for membrane fusion.³² A similar mechanism may be also responsible for the penetration of the S2 subunit into the natural PS film. Moreover, it has been reported that the FP-mediated fusion became more favorable for membranes containing cholesterol³³ and negatively charged phospholipids,³⁴ likely due to electrostatic interactions promoted by the positively charged FP. The natural PS contains 20% anionic phospholipids, including phosphatidylglycerol, phosphatidylinositol, and lysophosphatidic acid, and up to 10% cholesterol.8 Hence, the FP-mediated fusion is expected to prevail in the natural PS film.

Nevertheless, it should be noted that the surfactant preparation used in this study, that is, Infasurf, is devoid of the hydrophilic surfactant proteins SP-A and SP-D.²⁴ It is known that these immunological proteins, especially SP-D, modulate viral infection in the lung. It has been shown that a recombinant fragment of human SP-D inhibits replication and infection of SARS-CoV-2.¹⁰ However, the molecular mechanism appears to be mostly related to the SP-D-mediated interaction between the S1 subunit of SARS-CoV-2 and the ACE2 receptor of the host cells.¹⁰ Hence, lack of hydrophilic surfactant proteins in Infasurf does not likely vary our conclusions about the S2 subunit-mediated domain fusion found in natural PS films.

Using combined biophysical simulations and AFM imaging, we have studied the biophysical impact of the S2 subunit on a natural PS film, Infasurf. We have concluded that the S2 subunit can inhibit the biophysical properties of the PS. We have provided direct experimental evidence for S2 subunit-induced microdomain fusion in the Infasurf monolayer. The surfactant inhibition has been attributed to the membrane fluidization caused by insertion of the S2 subunit mediated by its fusion peptide. These findings may provide novel insight into the understanding of biophysical mechanisms responsible for PS interactions with SARS-CoV-2 and may have translational implications in the further development of surfactant replacement therapy for COVID-19 patients.

ASSOCIATED CONTENT

Solution Supporting Information

The Supporting Information is available free of charge at https://pubs.acs.org/doi/10.1021/acs.jpclett.2c01998.

Experimental Section. Reproducibility of the biophysical impact of the S2 subunit on Infasurf. Compression isotherms with increasing compression rate and higher S2 subunit concentration. Adsorption kinetics and equilibrium surface tension of the S2 subunit. Reproducibility of the S2 subunit mediated domain fusion determined with AFM imaging (PDF)

AUTHOR INFORMATION

Corresponding Author

Yi Y. Zuo — Department of Mechanical Engineering, University of Hawaii at Manoa, Honolulu 96822 Hawaii, United States; Department of Pediatrics, John A. Burns School of Medicine, University of Hawaii, Honolulu 96826 Hawaii, United States; orcid.org/0000-0002-3992-3238; Phone: 808-956-9650; Email: yzuo@hawaii.edu; Fax: 808-956-2373

Authors

Xiaojie Xu — Department of Mechanical Engineering, University of Hawaii at Manoa, Honolulu 96822 Hawaii, United States

Guangle Li — Department of Mechanical Engineering, University of Hawaii at Manoa, Honolulu 96822 Hawaii, United States

Bingbing Sun – State Key Laboratory of Fine Chemicals and School of Chemical Engineering, Dalian University of Technology, Dalian 116024, China

Complete contact information is available at: https://pubs.acs.org/10.1021/acs.jpclett.2c01998

Author Contributions

These authors contributed equally to this work.

Notes

The authors declare no competing financial interest.

■ ACKNOWLEDGMENTS

We thank Dr. S. Row of ONY Biotech for the donation of Infasurf samples. This research was supported by the National Science Foundation Grant No. CBET-2011317 (Y.Y.Z.).

REFERENCES

(1) Yao, H.; Song, Y.; Chen, Y.; Wu, N.; Xu, J.; Sun, C.; Zhang, J.; Weng, T.; Zhang, Z.; Wu, Z.; Cheng, L.; Shi, D.; Lu, X.; Lei, J.;

- Crispin, M.; Shi, Y.; Li, L.; Li, S. Molecular Architecture of the SARS-CoV-2 Virus. *Cell* **2020**, *183* (3), 730–738.
- (2) Hoffmann, M.; Kleine-Weber, H.; Schroeder, S.; Krüger, N.; Herrler, T.; Erichsen, S.; Schiergens, T. S.; Herrler, G.; Wu, N.-H.; Nitsche, A.; Müller, M. A.; Drosten, C.; Pöhlmann, S. SARS-CoV-2 Cell Entry Depends on ACE2 and TMPRSS2 and Is Blocked by a Clinically Proven Protease Inhibitor. *Cell* **2020**, *181* (2), 271–280.
- (3) Turonova, B.; Sikora, M.; Schurmann, C.; Hagen, W. J. H.; Welsch, S.; Blanc, F. E. C.; von Bulow, S.; Gecht, M.; Bagola, K.; Horner, C.; van Zandbergen, G.; Landry, J.; de Azevedo, N. T. D.; Mosalaganti, S.; Schwarz, A.; Covino, R.; Muhlebach, M. D.; Hummer, G.; Krijnse Locker, J.; Beck, M. In situ structural analysis of SARS-CoV-2 spike reveals flexibility mediated by three hinges. *Science* 2020, 370 (6513), 203–208.
- (4) Ou, X.; Liu, Y.; Lei, X.; Li, P.; Mi, D.; Ren, L.; Guo, L.; Guo, R.; Chen, T.; Hu, J.; Xiang, Z.; Mu, Z.; Chen, X.; Chen, J.; Hu, K.; Jin, Q.; Wang, J.; Qian, Z. Characterization of spike glycoprotein of SARS-CoV-2 on virus entry and its immune cross-reactivity with SARS-CoV. *Nat. Commun.* **2020**, *11* (1), 1620.
- (5) Jackson, C. B.; Farzan, M.; Chen, B.; Choe, H. Mechanisms of SARS-CoV-2 entry into cells. *Nat. Rev. Mol. Cell Biol.* **2022**, 23 (1), 3–20.
- (6) Meyer, N. J.; Gattinoni, L.; Calfee, C. S. Acute respiratory distress syndrome. *Lancet* **2021**, 398 (10300), 622-637.
- (7) Hamming, I.; Timens, W.; Bulthuis, M.; Lely, A.; Navis, G.; van Goor, H. Tissue distribution of ACE2 protein, the functional receptor for SARS coronavirus. A first step in understanding SARS pathogenesis. *Journal of Pathology* **2004**, 203 (2), 631–637.
- (8) Zuo, Y. Y.; Veldhuizen, R. A. W.; Neumann, A. W.; Petersen, N. O.; Possmayer, F. Current perspectives in pulmonary surfactant Inhibition, enhancement and evaluation. *Biochimica et Biophysica Acta* (BBA) Biomembranes 2008, 1778 (10), 1947–1977.
- (9) Hsieh, M.-H.; Beirag, N.; Murugaiah, V.; Chou, Y.-C.; Kuo, W.-S.; Kao, H.-F.; Madan, T.; Kishore, U.; Wang, J.-Y. Human Surfactant Protein D Binds Spike Protein and Acts as an Entry Inhibitor of SARS-CoV-2 Pseudotyped Viral Particles. *Front. Immunol.* **2021**, *12*. DOI: 10.3389/fimmu.2021.641360
- (10) Madan, T.; Biswas, B.; Varghese, P. M.; Subedi, R.; Pandit, H.; Idicula-Thomas, S.; Kundu, I.; Rooge, S.; Agarwal, R.; Tripathi, D. M.; Kaur, S.; Gupta, E.; Gupta, S. K.; Kishore, U. A Recombinant Fragment of Human Surfactant Protein D Binds Spike Protein and Inhibits Infectivity and Replication of SARS-CoV-2 in Clinical Samples. *American journal of respiratory cell and molecular biology* **2021**, *65* (1), 41–53.
- (11) Schousboe, P.; Ronit, A.; Nielsen, H. B.; Benfield, T.; Wiese, L.; Scoutaris, N.; Verder, H.; Berg, R. M. G.; Verder, P.; Plovsing, R. R. Reduced levels of pulmonary surfactant in COVID-19 ARDS. *Sci. Rep.* **2022**, *12* (1), 4040.
- (12) Zuo, Y. Y.; Uspal, W. E.; Wei, T. Airborne Transmission of COVID-19: Aerosol Dispersion, Lung Deposition, and Virus-Receptor Interactions. ACS Nano 2020, 14 (12), 16502–16524.
- (13) Herman, L.; De Smedt, S. C.; Raemdonck, K. Pulmonary surfactant as a versatile biomaterial to fight COVID-19. *Journal of controlled release: official journal of the Controlled Release Society* **2022**, 342, 170–188.
- (14) Veldhuizen, R. A. W.; Zuo, Y. Y.; Petersen, N. O.; Lewis, J. F.; Possmayer, F. The COVID-19 pandemic: a target for surfactant therapy? *Expert review of respiratory medicine* **2021**, *15* (5), 597–608.
- (15) Piva, S.; DiBlasi, R. M.; Slee, A. E.; Jobe, A. H.; Roccaro, A. M.; Filippini, M.; Latronico, N.; Bertoni, M.; Marshall, J. C.; Portman, M. A. Surfactant therapy for COVID-19 related ARDS: a retrospective case—control pilot study. *Respiratory Research* **2021**, 22 (1), 20.
- (16) Heching, M.; Lev, S.; Shitenberg, D.; Dicker, D.; Kramer, M. R. Surfactant for the Treatment of ARDS in a Patient With COVID-19. *CHEST* **2021**, *160* (1), e9—e12.
- (17) Cai, Y.; Zhang, J.; Xiao, T.; Peng, H.; Sterling, S. M.; Walsh, R. M.; Rawson, S.; Rits-Volloch, S.; Chen, B. Distinct conformational states of SARS-CoV-2 spike protein. *Science* **2020**, *369* (6511), 1586–1592.

- (18) Chakraborty, H.; Bhattacharjya, S. Mechanistic insights of host cell fusion of SARS-CoV-1 and SARS-CoV-2 from atomic resolution structure and membrane dynamics. *Biophys. Chem.* **2020**, *265*, 106438.
- (19) Gorgun, D.; Lihan, M.; Kapoor, K.; Tajkhorshid, E. Binding mode of SARS-CoV-2 fusion peptide to human cellular membrane. *Biophysical journal* **2021**, *120* (14), 2914–2926.
- (20) Schaefer, S. L.; Jung, H.; Hummer, G. Binding of SARS-CoV-2 Fusion Peptide to Host Endosome and Plasma Membrane. *J. Phys. Chem. B* **2021**, *125* (28), *7732–7741*.
- (21) Valle, R. P.; Wu, T.; Zuo, Y. Y. Biophysical Influence of Airborne Carbon Nanomaterials on Natural Pulmonary Surfactant. *ACS Nano* **2015**, 9 (5), 5413–5421.
- (22) Xu, L.; Yang, Y.; Zuo, Y. Y. Atomic Force Microscopy Imaging of Adsorbed Pulmonary Surfactant Films. *Biophysical journal* **2020**, 119 (4), 756–766.
- (23) Bachofen, H.; Schurch, S.; Urbinelli, M.; Weibel, E. R. Relations among alveolar surface tension, surface area, volume, and recoil pressure. *J. Appl. Physiol.* **1987**, 62 (5), 1878–1887.
- (24) Zhang, H.; Fan, Q.; Wang, Y. E.; Neal, C. R.; Zuo, Y. Y. Comparative study of clinical pulmonary surfactants using atomic force microscopy. *Biochimica et biophysica acta* **2011**, *1808* (7), 1832–42.
- (25) Keating, E.; Zuo, Y. Y.; Tadayyon, S. M.; Petersen, N. O.; Possmayer, F.; Veldhuizen, R. A. A modified squeeze-out mechanism for generating high surface pressures with pulmonary surfactant. *Biochimica et biophysica acta* **2012**, *1818* (5), 1225–34.
- (26) Zhang, H.; Wang, Y. E.; Fan, Q.; Zuo, Y. Y. On the Low Surface Tension of Lung Surfactant. *Langmuir* **2011**, 27 (13), 8351–8358.
- (27) Yang, S.-T.; Kiessling, V.; Tamm, L. K. Line tension at lipid phase boundaries as driving force for HIV fusion peptide-mediated fusion. *Nat. Commun.* **2016**, 7 (1), 11401.
- (28) Risselada, H. J.; Marelli, G.; Fuhrmans, M.; Smirnova, Y. G.; Grubmüller, H.; Marrink, S. J.; Müller, M. Line-Tension Controlled Mechanism for Influenza Fusion. *PLoS One* **2012**, *7* (6), No. e38302.
- (29) Xia, S.; Zhu, Y.; Liu, M.; Lan, Q.; Xu, W.; Wu, Y.; Ying, T.; Liu, S.; Shi, Z.; Jiang, S.; Lu, L. Fusion mechanism of 2019-nCoV and fusion inhibitors targeting HR1 domain in spike protein. *Cellular & Molecular Immunology* **2020**, *17* (7), 765–767.
- (30) Castillo-Sánchez, J. C.; Cruz, A.; Pérez-Gil, J. Structural hallmarks of lung surfactant: Lipid-protein interactions, membrane structure and future challenges. *Arch. Biochem. Biophys.* **2021**, 703, 108850.
- (31) Marsh, D. Lateral pressure in membranes. *Biochimica et biophysica acta* **1996**, 1286 (3), 183–223.
- (32) Koppisetti, R. K.; Fulcher, Y. G.; Van Doren, S. R. Fusion Peptide of SARS-CoV-2 Spike Rearranges into a Wedge Inserted in Bilayered Micelles. *J. Am. Chem. Soc.* **2021**, *143* (33), 13205–13211.
- (33) Santamaria, A.; Batchu, K. C.; Matsarskaia, O.; Prévost, S. F.; Russo, D.; Natali, F.; Seydel, T.; Hoffmann, I.; Laux, V.; Haertlein, M.; Darwish, T. A.; Russell, R. A.; Corucci, G.; Fragneto, G.; Maestro, A.; Zaccai, N. R. Strikingly Different Roles of SARS-CoV-2 Fusion Peptides Uncovered by Neutron Scattering. *J. Am. Chem. Soc.* **2022**, 144 (7), 2968–2979.
- (34) Guillén, J.; Almeida, R. F. M. d.; Prieto, M.; Villalaín, J. Structural and Dynamic Characterization of the Interaction of the Putative Fusion Peptide of the S2 SARS-CoV Virus Protein with Lipid Membranes. *J. Phys. Chem. B* **2008**, *112* (23), 6997–7007.